

PATTERN FORMATION IN BACTERIAL COLONIES WITH
DENSITY-DEPENDENT DIFFUSION

by

Julien Smith-Roberge

Submitted in partial fulfillment of the requirements
for the degree of Master of Science

at

Dalhousie University
Halifax, Nova Scotia
April 2017

© Copyright by Julien Smith-Roberge, 2017

Table of Contents

List of Figures	iii
Abstract	iv
Acknowledgements	v
Chapter 1 Introduction	1
Chapter 2 Model	4
2.1 Turing Instability	5
Chapter 3 Exact and Approximate Solutions	7
3.1 Non-constant Stationary Solutions	7
3.2 Solutions for $\tau_p = 0$ and Small D_h	10
3.3 Stationary Solutions for Large Values of $s(h)$	12
3.4 Solutions for Large $s(h)$, Small D_h , and $\tau_p = 0$	14
Chapter 4 Stability	16
4.1 Linearization and an Eigenvalue Problem	16
4.2 Jump Conditions via Integration	17
4.3 Jump Conditions via Linearization	18
4.4 Solutions to the Eigenvalue Problem for Large $s(h)$ Values	20
4.5 Revisiting Stability in the Small D_h , $\tau_p = 0$ Regime	24
Chapter 5 Discussion	28
Bibliography	30
Appendix A FlexPDE Code	32

List of Figures

Figure 1.1	Evolution of the perturbed homogeneous steady-state, with structure becoming noticeable at $t \approx 0.5$	2
Figure 1.2	Evolution of the shifted steady state in the stable regime ($D_h = 0.195$). The red line tracks the motion of the interface.	3
Figure 1.3	Evolution of the shifted steady state in the unstable regime ($D_h = 0.203$). The red line tracks the motion of the interface. The interface is eventually destroyed.	3
Figure 3.1	Numerically calculated solutions vs the piecewise constant approximation. The full solution is displayed on the left, while the right shows the scale of the error. Parameters are $D_h = 0.005$, $D_+ = 500$, and $D_- = 1000$. To facilitate numerical calculation, $s(h)$ was approximated by a sharp sigmoid curve.	9
Figure 3.2	motion of the front as predicted by the ODE (in black) compared to simulation results (red crosses). Parameter values are $D_h = 0.005$, $D_+ = 500$, $D_- = 1000$	15
Figure 4.1	Plotting the real part of the first two eigenvalues as a function of D_h , with $s_0 = 0.5$. Notice as D_h becomes large, the first eigenvalue grows very quickly. This apparent asymptote corresponds to the onset of non-existence of single-jump solutions. At intermediate D_h values the first two roots become a complex pair, and the system undergoes a Hopf bifurcation. For small D_h values, the first two roots are again real, but remain negative.	22
Figure 4.2	Plots comparing the motion of x_0 in the linearly stable ($D_h = 0.199$, top) and linearly unstable ($D_h = 0.202$, bottom) regimes, with $D_+ = 500$ and $D_- = 1000$ in both cases, and $s(h)$ approximated by a sharp sigmoid curve. In each plot, the steady-state solution was perturbed, and the location of x_0 tracked as the solution evolved. In the stable case, the location of x_0 exhibits damped oscillations consistent with the predicted eigenvalues. In the unstable case, the oscillations grow until x_0 drifts to the edge of the domain, at which point the solution collapses to an approximately constant and homogeneous profile ($t \approx 45$). This is followed by repeated spontaneous emergence of structure via Turing instability, punctuated by collapse to a nearly constant solution.	23

Abstract

Recent experiments have shown that patterns can emerge in bacterial colonies programmed to have a drop in diffusion when population densities (detected via a quorum sensing mechanism) are sufficiently large. We examine one partial differential equation model of this system, and construct its non-constant stationary solutions. We demonstrate analytically that these solutions are stable when the diffusion rate of bacteria is large and the diffusion rate of signalling molecules, D_h , is small. We further demonstrate that increasing D_h induces a Hopf bifurcation, resulting in a loss of stability. These results are confirmed by numerical simulations.

Acknowledgements

I would like to thank Dr. Theodore Kolokolnikov and Dr. David Iron, without whom none of this work would have been possible.

Chapter 1

Introduction

Several species of bacteria move via a run and tumble mechanism—motion in a straight line (runs) punctuated by periods of random reorientation (tumbles)—which, for sufficiently large populations, can be modelled as diffusion. Moreover, by changing the ratio of runs to tumbles, a population can effectively change its diffusion rate. Such a change can give rise to chemotaxis and other types of non-linear diffusion, each of which may lead to the formation of patterns or other group behaviour [1]. Explaining such phenomena naturally leads to the development of mathematical models. Perhaps the best known of these is the Keller-Segel model [2], though the literature is replete with examples of reaction-diffusion type models where simple diffusion has been replaced by some nonlinear variant [3–11].

The bacterial species *Vibrio fischeri* secretes acyl-homoserine lactone (AHL), a signalling molecule which acts as part of a quorum sensing mechanism [12]. When large populations of *V. fischeri* gather in one place, the concentration of AHL can reach sufficiently high levels to trigger changes in the behaviour of the bacteria. In the wild, this particular mechanism allows the bacteria to regulate bioluminescence. Similar quorum sensing mechanisms abound in nature [12]. Using techniques from synthetic biology, Liu *et al.* [13] introduced this mechanism to a strain of *E. coli*, and coupled it to a pathway which controls run-and-tumble motility. The net effect is for the bacteria to have a sudden drop in diffusion when population density is large enough for the AHL concentration to surpass a given threshold. Similar population-dependent changes in diffusion are known to generate patterns [14–16]. Further experiments showed that these modified bacteria form patterns when grown on agar plates. The group proposed two partial differential equation (PDE) models to help explain this behaviour [13, 17].

This thesis constitutes an exploration of one of these models, in particular its non-trivial steady states and their stability. We begin with an analysis of the linear

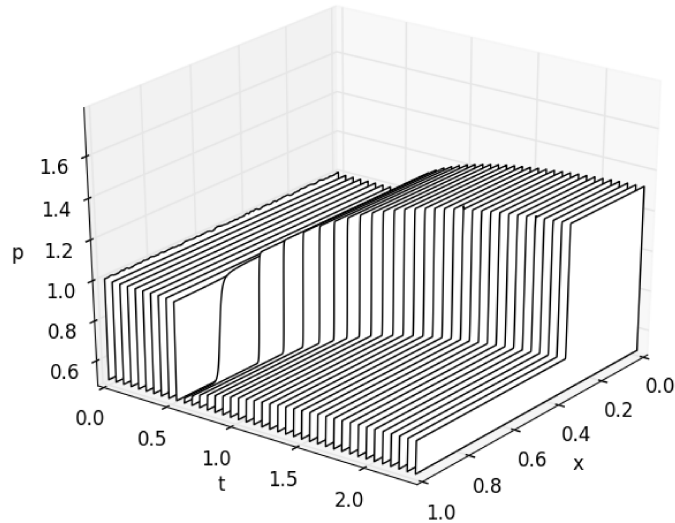


Figure 1.1: Evolution of the perturbed homogeneous steady-state, with structure becoming noticeable at $t \approx 0.5$.

stability of the constant steady-state, and show that the system can be tuned to exhibit a Turing instability (see figure 1.1). From there, we explicitly construct non-constant steady-state solutions, and derive an approximate solution for the case where the bacterial diffusion rate is large. These solutions contain jump discontinuities. We derive an equation of motion for a single discontinuity in the case where the diffusion of signalling molecules, D_h , is small. Using the aforementioned approximate solution, we further show that this equation of motion has a stable steady-state when bacterial diffusion is large by explicitly computing its spectrum (see section 3.4).

In the second half of the thesis, we address the question of stability more generally. We use linear stability analysis to formulate the associated eigenvalue problem, and derive a transcendental equation which has the eigenvalues as its roots. Solving this equation numerically, we show that the system exhibits a Hopf bifurcation (see figures 1.2 and 1.3). We conclude by showing that the linear stability analysis reproduces the eigenvalue derived via the equation of motion.

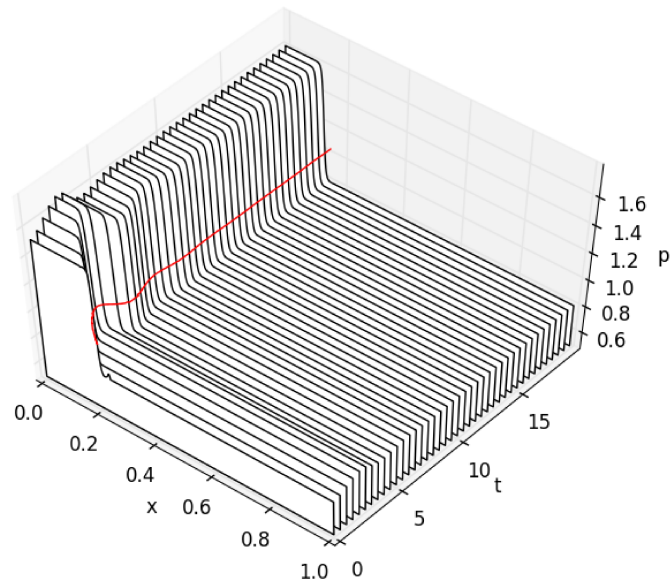


Figure 1.2: Evolution of the shifted steady state in the stable regime ($D_h = 0.195$). The red line tracks the motion of the interface.

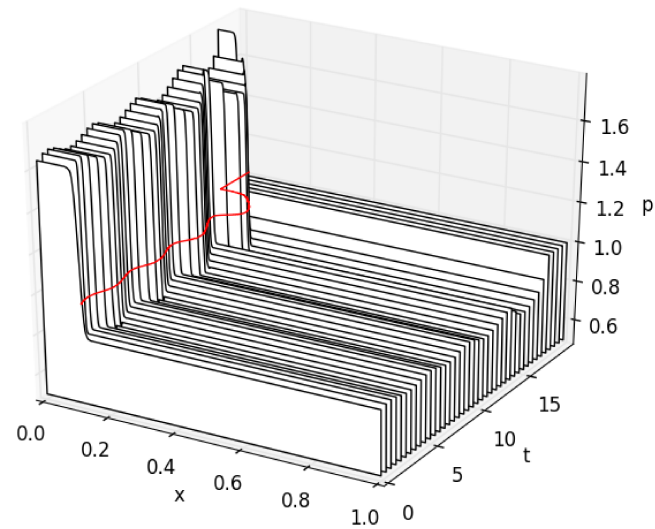


Figure 1.3: Evolution of the shifted steady state in the unstable regime ($D_h = 0.203$). The red line tracks the motion of the interface. The interface is eventually destroyed.

Chapter 2

Model

The model in question is a one-dimensional non-linear PDE system:

$$\begin{aligned}\tau_p p_t &= (s(h)p)_{xx} + \gamma p \left(1 - \frac{p}{p_s}\right), \\ \tau_h h_t &= D_h h_{xx} + \alpha p - \beta h.\end{aligned}$$

We use subscripts \cdot_t and \cdot_x to denote partial derivatives w.r.t. x and t (all other subscripts act purely as identifying markers), and $'$ to denote the derivative of a function of one variable. The quantities $p(x, t)$ and $h(x, t)$ measure the density of bacteria and AHL respectively. AHL is produced by the bacteria at a rate α , and decays at a rate β . The constants γ and p_s represent, respectively, the logistic growth rate and equilibrium population of the bacteria.

We may rescale $\hat{p} = \frac{p}{p_s}$, and divide the equation for p by γp_s to obtain $\frac{\tau_p}{\gamma} \hat{p}_t = \left(\frac{s(h)}{\gamma} \hat{p}\right)_{xx} + \hat{p}(1 - \hat{p})$. We can perform a similar procedure on the equation for h : first dividing through by the coefficient in front of \hat{p} , then rescaling $\hat{h} = \frac{\beta}{\alpha p_s} h$ to eliminate the multiplicative constants in the $-h$ term. This leaves us with two groupings of constants in the h equation. By choosing appropriate scaling for the time, we may eliminate the group in front of h_t . By grouping constants and relabeling, we recover a simplified model. This rescaling is equivalent to choosing $\gamma = p_s = \beta = \alpha = \tau_h = 1$ (as in equations 2.1 and 2.2).

D_h is the diffusion rate for h , whereas diffusion of p depends on the value of h via a function s . Unless otherwise stated, we will take s to be piecewise constant, though it will occasionally be useful to replace it by a sharp sigmoid (for example, almost all numerical results are calculated using a sigmoid for s). At low h concentration, bacteria diffuse freely. High h concentrations, however, trigger the synthetic genetic

circuit described in the introduction, inducing a drop in the diffusion rate of the bacteria. This drop in diffusion happens at some critical AHL concentration, h_c .

These equations are solved on a finite domain, which, by choosing the correct scaling, we may take to be the unit interval, $[0, 1]$. We impose no-flux boundary conditions for both p and h . The system has a trivial constant solution, $p(x, t) = 1$, $h(x, t) = 1$. If we take s to be a sigmoid, we may carry out linear stability analysis (see below). Such analysis shows that this solution becomes unstable when $s'(1)$ is negative and sufficiently large (i.e. s is a very sharp sigmoid curve switching values at $h = 1$). This motivates us to chose $h_c = 1$.¹

2.1 Turing Instability

We consider the following system

$$\tau_p p_t = (s(h)p)_{xx} + p(1 - p) , \quad (2.1)$$

$$h_t = D_h h_{xx} + p - h , \quad (2.2)$$

where $s(h)$ is some sigmoid curve. To investigate the stability of the trivial steady-state solution ($p = h = 1$), we consider small perturbations of the homogeneous steady-state which take the form

$$p = 1 + e^{\lambda t} e^{imx} \phi ,$$

$$h = 1 + e^{\lambda t} e^{imx} \psi .$$

Approximating $s(h)p$ to first order around the steady state, we obtain

$$s(h)p \approx s(1) + s'(1)e^{\lambda t} e^{imx} \psi + s(1)e^{\lambda t} e^{imx} \phi .$$

Substitution into the original system, and ignoring higher order terms, we obtain

$$\tau_p \lambda \phi = -m^2 s'(1) \psi - m^2 s(1) \phi - \phi ,$$

$$\lambda \psi = -D_h m^2 \psi + \phi - \psi .$$

¹This does indeed mean that Turing-type instabilities only occur when the quorum sensing threshold is very close to the equilibrium AHL concentration. However, as described by [17], non-homogeneous patterns can occur through other mechanisms that don't necessitate such fine-tuning.

Or, written in matrix notation,

$$\lambda \begin{pmatrix} \phi \\ \psi \end{pmatrix} = \begin{pmatrix} -\frac{m^2 s(1)+1}{\tau_p} & -\frac{m^2 s'(1)}{\tau_p} \\ 1 & -D_h m^2 - 1 \end{pmatrix} \begin{pmatrix} \phi \\ \psi \end{pmatrix} .$$

Note that the trace of this matrix is $-\frac{m^2 s(1)+1}{\tau_p} - D_h m^2 - 1$, which is always negative. Therefore, if we wish to obtain positive eigenvalues (corresponding to an unstable solution), we require that the determinant also be negative. I.e.

$$(-m^2 s(1) - 1)(-D_h m^2 - 1) + m^2 s'(1) < 0 .$$

When m is large, the determinant is positive. A negative determinant, therefore, is equivalent to $(-m^2 s(1) - 1)(-D_h m^2 - 1) + m^2 s'(1)$ having distinct real roots when considered as a polynomial in m^2 . Expanding yields

$$s(1)D_h m^4 + (D_h + s(1) + s'(1))m^2 + 1 .$$

So we look for parameter values that give a positive discriminant and a negative m^2 term (since we want this polynomial to take on negative values when $m^2 > 0$). This is summarized in the following proposition.

Proposition 1. *The steady-state solution $p(x, t) = h(x, t) = 1$ to equations (2.1) and (2.2) is*

- *linearly unstable if $D_h < -s'(1) - s(1)$ and $(D_h + s(1) + s'(1))^2 - 4s(1)D_h > 0$*
- *linearly stable otherwise.*

These conditions can be simplified ever further by noting that, in the case where $s(h)$ is a sigmoid, we need only require that $s(h)$ is decreasing rapidly at one. I.e. $s'(1)$ is large and negative.

Chapter 3

Exact and Approximate Solutions

As with many non-linear PDE, general solutions are beyond our grasp. We begin with a selection of solutions for special cases. Our analysis will focus primarily on stationary and near-stationary solutions, and, beyond what has already been said about Turing instability, we will largely ignore the details behind a solution's transition from a nearly constant profile to one with large-scale inhomogeneities.

3.1 Non-constant Stationary Solutions

We look for stationary solutions to equations (2.1) and (2.2),

$$\begin{aligned}\tau_p p_t &= (s(h)p)_{xx} + p(1-p) , \\ h_t &= D_h h_{xx} + p - h ,\end{aligned}$$

where we now define s to be

$$s(h) = \begin{cases} D_- & h \leq 1 \\ D_+ & h > 1 \end{cases} ,$$
$$D_- > D_+ .$$

We can partition the domain into subintervals based on the value of h , such that s is constant on each interval, switching value between D_+ and D_- at the boundaries. Thus, the problem reduces to solving Fisher's equation on each interval, subject to some boundary conditions (see below). i.e. the stationary solutions for p will satisfy either $D_+ p_{xx} = -p(1-p)$ or $D_- p_{xx} = -p(1-p)$ on any of these intervals.

This ordinary differential equation (ODE) has solutions of the form $a + b \operatorname{sn}^2(c(x + x_0); m)$, where $\operatorname{sn}(x; m)$ is a Jacobi elliptic function. [18] Substitution into one of these

ODEs (without loss of generality, pick the one containing D_+) yields three constraints,

$$\begin{aligned} 0 &= 3a^2m + 2ab(1 + m) + b^2 , \\ 0 &= \frac{-4c^2D_+}{b}(3am + bm + b) + 1 , \\ 0 &= \frac{6c^2mD_+}{b} - 1 , \end{aligned}$$

leaving the expected two degrees of freedom.

We can solve for h using variation of parameters. This yields solutions in terms of antiderivatives involving sn^2 which can, at best, be expressed as an infinite series. While these solutions are correct, they offer little insight into the behaviour of the system, and quickly become unwieldy. This will eventually motivate us to look for approximate solutions. Before we do so, we must determine how solutions behave at points where $h = 1$.

Suppose x_0 is one such point, and assume for the sake of notation that $s(h) = D_+$ to the right of x_0 , and $s(h) = D_-$ to the left. Integrating (2.1) in a small neighbourhood around x_0 , we obtain

$$\begin{aligned} 0 &= \int_{x_0^-}^{x_0^+} (s(h)p)_{xx} dx + \int_{x_0^-}^{x_0^+} p(1-p) dx \\ &= D_+ p_x(x_0^+, t) - D_- p_x(x_0^-, t) . \end{aligned} \tag{3.1}$$

Similarly, premultiplying (2.1) by x before integrating yields

$$0 = D_+ p(x_0^+, t) - D_- p(x_0^-, t) . \tag{3.2}$$

From this, we see that p will have a discontinuity at x_0 (see figure 3.1). The same calculation can be done for equation (2.2) to obtain the following conditions:

$$0 = h_x(x_0^+, t) - h_x(x_0^-, t) , \tag{3.3}$$

$$1 = h(x_0^+, t) = h(x_0^-, t) . \tag{3.4}$$

These four constraints will be collectively referred to as jump conditions, since p will have a jump discontinuity at each point where $h = 1$. For a given a number

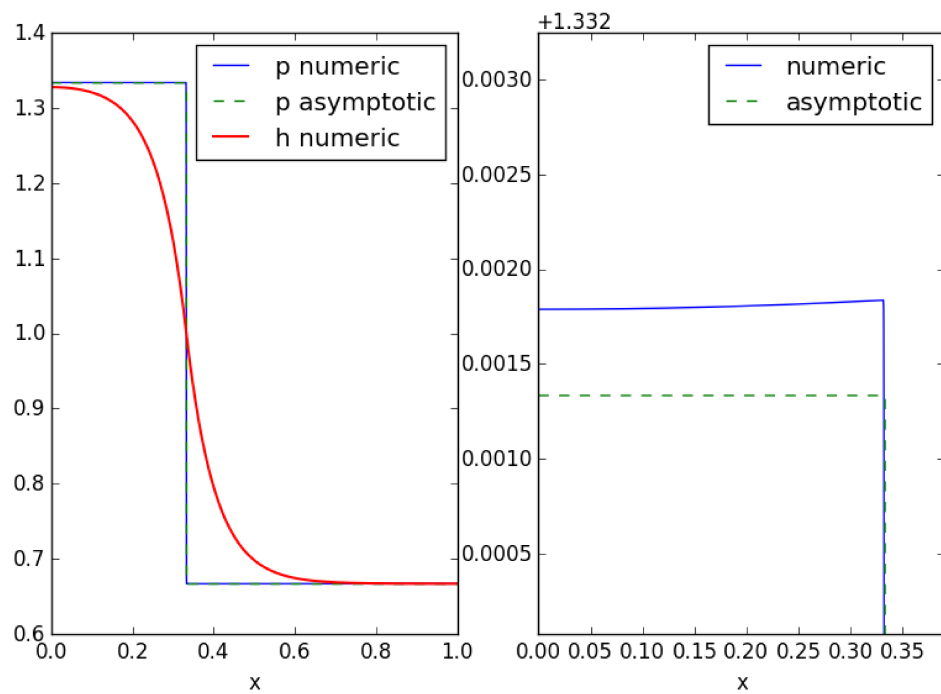
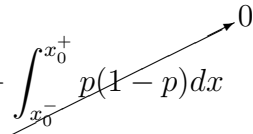


Figure 3.1: Numerically calculated solutions vs the piecewise constant approximation. The full solution is displayed on the left, while the right shows the scale of the error. Parameters are $D_h = 0.005$, $D_+ = 500$, and $D_- = 1000$. To facilitate numerical calculation, $s(h)$ was approximated by a sharp sigmoid curve.

of jumps, the jump conditions and the no-flux boundary conditions give us enough constraints to determine a unique stationary solution. Note, however, that there is nothing to determine the number of jumps (in general this will depend on the initial conditions of the system), or to guarantee that a stationary solution exists that satisfies all the constraints (we will see an example of this non-existence later). We may, however, concatenate copies of a stationary solution to construct a new solution on a larger domain. With this in mind, the rest of this thesis will focus on solutions with a single jump discontinuity.

While these jump conditions hold for stationary solutions, non-stationary solutions may have moving discontinuities. This will amount to a Dirac delta appearing in the p_t term in equation (2.1), which will contribute an additional term when we integrate around $x_0(t)$. To account for this, we will re-integrate the equation for more carefully. Suppose p takes the form $p = A(t)H(x - x_0(t)) + \hat{p}(x, t)$, where $x_0(t)$ is the location of the interface, H is a Heaviside function, and $\hat{p}(x, t)$ is continuous.

$$\begin{aligned} \tau_p \int_{x_0^-}^{x_0^+} p_t dx &= \int_{x_0^-}^{x_0^+} (sp)_{xx} dx + \int_{x_0^-}^{x_0^+} p(1-p) dx \\ -\tau_p A(t)x_0'(t) &= sp_x \Big|_{x_0^-}^{x_0^+} \end{aligned} \tag{3.5}$$


We can verify that the other three conditions remain unchanged.

3.2 Solutions for $\tau_p = 0$ and Small D_h

We now turn our attention to approximate solutions with one jump discontinuity. Setting $\tau_p = 0$, we recover the PDE for stationary p . We will not, however, assume the system as a whole is stationary. Consequently, p depends on time implicitly via the position of the jump discontinuity, $x_0(t)$. Since the exact solution for h does not lend itself to easy algebraic manipulation, we limit our consideration to the small diffusion case, $0 < \varepsilon^2 = D_h \ll 1$.

Solutions for h are obtained by matching approximate solutions constructed near $x_0(t)$ and away from $x_0(t)$. Away from $x_0(t)$, diffusion is very small, and so h is approximately equal to p (see figure 3.1). To determine the behaviour of h around

$x_0(t)$, we introduce a new variable, $y = \frac{x}{\varepsilon}$, such that $\varepsilon^2 h_{xx} = h_{yy}$. We also assume h takes the form of a moving profile, $h = h(x - x_0(t))$. This allows us to write $h_t = -h'(x - x_0(t))x'_0(t) = -\frac{x'_0}{\varepsilon}h_y$. We also define $s := \varepsilon t$, and $\hat{x}_0(s) := x_0(t)$, allowing us to make the substitution $\hat{x}'_0(s) = \frac{x'_0(t)}{\varepsilon}$. Thus, the second PDE in the system becomes

$$-\hat{x}'_0 h_y = h_{yy} + p - h .$$

In order to match with the solution away from $x_0(t)$, we require that $h \rightarrow p$ as $y \rightarrow \pm\infty$ (note: under this change of variable, p is approximately piecewise constant w.r.t. y). We also require that the jump conditions be satisfied at $x_0(t)$ (i.e.: $h = 1$ and h' is continuous).

Solutions for h are defined piecewise on either side of the jump, and take the form $h = p + c_1 e^{r_1 y} + c_2 e^{r_2 y}$, where r_1 and r_2 are roots of the characteristic equation $0 = x^2 + \hat{x}'_0 x - 1$, ordered such that $r_1 > 0 > r_2$. We will use the subscripts l and r to denote solutions to the left and right of $x_0(t)$.¹ Applying the limiting conditions on the left, we have $h_l = p_l + c_1 e^{r_1 y}$. Similarly, on the right, $h_r = p_r + c_2 e^{r_2 y}$. The jump conditions (3.3) and (3.4) at $x_0(t)$ simplify to

$$\begin{aligned} p_l + c_1 e^{r_1 y} &= p_r + c_2 e^{r_2 y} = 1 , \\ c_1 r_1 e^{r_1 y} &= c_2 r_2 e^{r_2 y} . \end{aligned}$$

Multiplying the first equation by r_1 and subtracting the two, we obtain $r_1 p_l = r_1 p_r + (r_1 - r_2)c^2 e^{r_2 y} \implies \frac{p_l - p_r}{c^2 e^{r_2 y}} = \frac{r_1 - r_2}{r_1}$. And, recalling that $c^2 e^{r_2 y} = 1 - p_r$ at $x_0(t)$, we obtain a differential equation describing the motion of the interface:

$$\frac{p_l - p_r}{1 - p_r} = \frac{r_1 - r_2}{r_1} .$$

Solving the characteristic equation yields $r_1 = \frac{-\hat{x}'_0 + \sqrt{(\hat{x}'_0)^2 + 4}}{2}$ and $r_2 = \frac{-\hat{x}'_0 - \sqrt{(\hat{x}'_0)^2 + 4}}{2}$, so that

$$\frac{p_l - p_r}{1 - p_r} = \frac{2\sqrt{(\hat{x}'_0)^2 + 4}}{-\hat{x}'_0 + \sqrt{(\hat{x}'_0)^2 + 4}} .$$

¹This notation is used throughout the rest of the thesis.

Solving for $\hat{x}'_0(s)$, we obtain $\hat{x}'_0(s) = \frac{a-2}{\sqrt{a-1}}$, or, returning to the original time scale,

$$x'_0(t) = \varepsilon \frac{a-2}{\sqrt{a-1}},$$

where $a = \frac{p_l(x_0) - p_r(x_0)}{1 - p_r(x_0)}$.

In constructing an equation of motion for the jump, x_0 , we have effectively eliminated h from the system. The motion of x_0 doesn't depend explicitly on h , and all that is needed to specify the value of p is the location of x_0 . In principle, we have a complete description of the solution. In practice, constructing this solution requires that we solve a set of transcendental equations (recall that the exact solutions for p are in terms of Jacobi elliptic functions). However, we can obtain more explicit results if we assume D_+ and D_- are large.

3.3 Stationary Solutions for Large Values of $s(h)$

We again look for stationary solutions where $h = 1$ exactly once, but with the assumption that D_+ and D_- are both large. In this case, the diffusive term dominates, so $p(x)$ is approximately piecewise constant. Expanding $p(x)$ in terms of a Taylor series at either end of the domain, we obtain the following approximations

$$\begin{aligned} p_l(x) &= p_{l0} + p_{l2}x^2 && \text{for } x < x_0, \\ p_r(x) &= p_{r0} + p_{r2}(x-1)^2 && \text{for } x > x_0. \end{aligned}$$

Note, p_{l0} , p_{l2} , p_{r0} and p_{r2} are constants. Without loss of generality, assume $p_{l0} > p_{r0}$, i.e. $s(h) = D_+$ in the left of the domain, and let

$$s_0 := \frac{D_+}{D_-} < 1. \quad (3.6)$$

The jump conditions (3.1) and (3.2) can be approximated by

$$\frac{p_{r0}}{p_{l0}} = s_0 = \frac{p_{r2}(x_0 - 1)}{p_{l2}x_0}.$$

Substituting the approximations for p into (2.1) and assuming $p_t = 0$ yields two more conditions:

$$\begin{aligned} 0 &= 2D_+p_{l2} + p_{l0}(1 - p_{l0}), \\ 0 &= 2D_-p_{r2} + p_{r0}(1 - p_{r0}). \end{aligned}$$

From these equations we can derive

$$s_0 \frac{x_0 - L}{x_0} = \frac{p_{l0} - 1}{p_{r0} - 1} \quad (3.7)$$

and

$$p_{l0} = \frac{s_0 x_0 - s_0 - x_0}{s_0^2 x_0 - s_0^2 - x_0} . \quad (3.8)$$

Taking the leading order approximation for p in the left of the domain and assuming h is stationary, equation (2.2) reduces to

$$0 = D_h h_{xx} + p_{l0} - h .$$

Thus $h_l = p_{l0} + c_1 \cosh\left(\sqrt{\frac{1}{D_h}}x\right)$, where c_1 is some undetermined constant. Similarly, in the right of the domain $h_r = p_{r0} + c_2 \cosh\left(\sqrt{\frac{1}{D_h}}(x-1)\right)$.

The jump conditions for h are

$$\begin{aligned} 1 &= p_{l0} + c_1 \cosh\left(\sqrt{\frac{1}{D_h}}x_0\right) , \\ 1 &= p_{r0} + c_2 \cosh\left(\sqrt{\frac{1}{D_h}}(x_0-1)\right) , \\ c_1 \sinh\left(\sqrt{\frac{1}{D_h}}x_0\right) &= c_2 \sinh\left(\sqrt{\frac{1}{D_h}}(x_0-1)\right) . \end{aligned}$$

Substituting into (3.7), we obtain

$$s_0 \frac{x_0 - 1}{x_0} = \frac{\tanh\left(\sqrt{\frac{1}{D_h}}(x_0-1)\right)}{\tanh\left(\sqrt{\frac{1}{D_h}}x_0\right)} ,$$

where s_0 is defined as in (3.6).

Solving this equation determines the value of x_0 , which in turn determines both p and h . Notice, however, that this equation need not have nontrivial solutions in the interval $(0, 1)$. In particular, this happens when $s_0 < \tanh\left(\sqrt{\frac{1}{D_h}}\right)\sqrt{D_h}$. Since $s_0 < 1$, we can always find a D_h large enough such that this is true.

Conversely, when D_h is very small, $\frac{\tanh\left(\sqrt{\frac{1}{D_h}}(x_0-1)\right)}{\tanh\left(\sqrt{\frac{1}{D_h}}x_0\right)} \approx -1$ when $x_0 \in (0, 1)$. Thus, we expect that $x_0 = \frac{s_0}{s_0+1}$, $p_{l0} = \frac{2}{s_0+1}$, and $p_{r0} = \frac{2s_0}{s_0+1}$ in the small D_h regime (see figure 3.1).

In summary we have the following:

Proposition 2. *Suppose $D_+, D_- \gg 1$, and let $s_0 = \frac{D_+}{D_-}$. Then equations (2.1) and (2.2) admit a non-trivial steady-state solution where p takes the form*

$$p(x) = \begin{cases} \frac{s_0 x_0 - s_0 - x_0}{s_0^2 x_0 - s_0^2 - x_0} & x \leq x_0 \\ \frac{s_0^2 x_0 - s_0^2 - s_0 x_0}{s_0^2 x_0 - s_0^2 - x_0} & x > x_0 \end{cases},$$

where x_0 solves

$$s_0 \frac{x_0 - 1}{x_0} = \frac{\tanh\left(\sqrt{\frac{1}{D_h}}(x_0 - 1)\right)}{\tanh\left(\sqrt{\frac{1}{D_h}}x_0\right)}.$$

And in particular, if $D_h \ll 1$, then $x_0 = \frac{s_0}{s_0+1}$ and p simplifies to

$$p(x) = \begin{cases} \frac{2}{s_0+1} & x \leq x_0 \\ \frac{2s_0}{s_0+1} & x > x_0 \end{cases}$$

3.4 Solutions for Large $s(h)$, Small D_h , and $\tau_p = 0$

Combining the results from the two previous sections, we obtain

$$x_0'(t) = \sqrt{D_h} \frac{s_0(1 - x_0(t)) - x_0(t)}{\sqrt{s_0 x_0(t)(1 - x_0(t))}}.$$

As expected, this equation has one steady state at $x_0(t) = \frac{s_0}{s_0+1}$. The associated eigenvalue $\lambda = -\sqrt{D_h} \frac{(1+s_0)^2}{s_0}$ is negative, so we expect the solution to be stable. This is observed in numerical simulation. Moreover, the trajectory of $x_0(t)$ in simulation matches the behaviour predicted by the equation of motion (see figure 3.2).

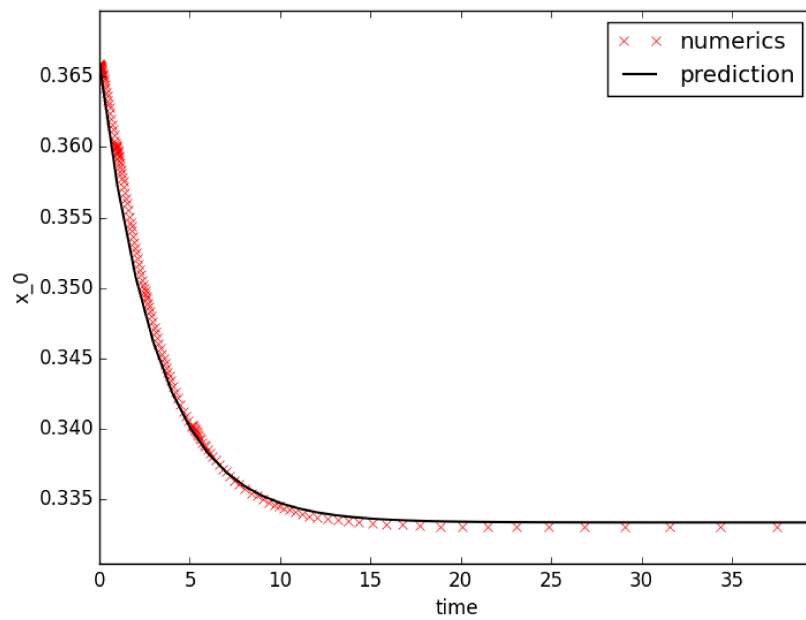


Figure 3.2: motion of the front as predicted by the ODE (in black) compared to simulation results (red crosses). Parameter values are $D_h = 0.005$, $D_+ = 500$, $D_- = 1000$.

Chapter 4

Stability

Thusfar, we have constructed exact and approximate solutions to the system of PDEs and shown that one of these solutions is stable. We now wish to address the question of stability in a more general context.

4.1 Linearization and an Eigenvalue Problem

Suppose that we have found some stationary solution, $p_s(x)$ and $h_s(x)$, to equations (2.1) and (2.2), and suppose that $h_s(x) = 1$ exactly once, at some point x_0 . We consider small perturbations of the form $p(x, t) = p_s(x) + \phi(x, t)$, and $h(x, t) = h_s(x) + \psi(x, t)$ where $\phi(x, t) \ll p_s(x)$ and $\psi(x, t) \ll h_s(x)$. Substituting into the PDEs and discarding higher order terms, we obtain the following linearized system:

$$\begin{aligned}\tau_p \phi_t(x, t) &= D_{\pm} \phi_{xx}(x, t) + \phi(x, t) (1 - 2p_s(x)) , \\ \psi_t(x, t) &= D_h \psi_{xx}(x, t) + \phi(x, t) - \psi(x, t) .\end{aligned}$$

Making the ansatz $\phi(x, t) = e^{\lambda t} \phi(x)$, $\psi(x, t) = e^{\lambda t} \psi(x)$, we obtain the following eigenvalue problem:

$$\lambda \tau_p \phi(x) = D_{\pm} \phi''(x) + \phi(x) (1 - 2p_s(x)) , \quad (4.1)$$

$$\lambda \psi(x) = D_h \psi''(x) + \phi(x) - \psi(x) . \quad (4.2)$$

The no-flux boundary conditions from the original system transfer trivially to the new functions, ϕ and ψ . Deriving jump conditions for the eigenvalue problem, however, requires more care. There are two ways to carry out the calculation: by integrating the equations across the jump, as we did for the original system, or by linearizing the original jump conditions. We begin with the former.

4.2 Jump Conditions via Integration

We assume that ϕ takes the form $\phi(x) = \hat{\phi}(x) + c\delta(x - x_0)$, where c is a constant, δ is a Dirac delta, and $\hat{\phi}$ is a (potentially discontinuous) function. We also assume ψ has no Dirac delta component.

Integrating (4.2) on a small interval around x_0 , we obtain

$$\begin{aligned} \lambda \int_{x_0^-}^{x_0^+} \psi dx &= D_h \int_{x_0^-}^{x_0^+} \psi_{xx} dx + \int_{x_0^-}^{x_0^+} \phi dx - \int_{x_0^-}^{x_0^+} \psi dx \\ 0 &= D_h \psi' \Big|_{x_0^-}^{x_0^+} + c . \end{aligned}$$

Premultiplying (4.2) by x and performing integration by parts, we derive

$$\begin{aligned} \lambda \int_{x_0^-}^{x_0^+} x \psi dx &= D_h \int_{x_0^-}^{x_0^+} x \psi_{xx} dx + \int_{x_0^-}^{x_0^+} x \phi dx - \int_{x_0^-}^{x_0^+} x \psi dx \\ 0 &= -x_0 c - D_h \psi \Big|_{x_0^-}^{x_0^+} + c x_0 \\ 0 &= \psi \Big|_{x_0^-}^{x_0^+} . \end{aligned}$$

Integrating (4.1) requires care in taking limits. Begin by integrating over $(x_0 - \Delta, x_0 + \Delta)$, where Δ is some small constant. We temporarily replace s by a sufficiently continuous sigmoid which switches value in some ε -neighbourhood around x_0 (i.e. $s(h)$ is approximately constant outside $(x_0 - \varepsilon, x_0 + \varepsilon)$). We observe that

$$s(h)p(x, t) \approx s(h_s)p_s(x) + p_s(x)s'(h_s)\psi(x)e^{\lambda t} + s(h_s)\phi(x)e^{\lambda t} ,$$

and adjust the linearization accordingly to obtain

$$\lambda \tau_p \phi(x) = (\psi(x)s'(h_s)p_s(x) + s(h_s)\phi(x))_{xx} + \phi(x)(1 - 2p_s(x)) . \quad (4.3)$$

After integrating, we will take the limit $\Delta \rightarrow 0$, and assume $\varepsilon \ll \Delta$. We also adopt the notation $f^+ := f(x_0^+)$, similarly for f^- .

Integrating (4.3) and taking the aforementioned limit yields

$$\begin{aligned}\tau_p \lambda \int_{x_0-\Delta}^{x_0+\Delta} \phi dx &= \int_{x_0-\Delta}^{x_0+\Delta} (\psi s'(h_s) p_s + s(h_s) \phi)_{xx} dx + \int_{x_0-\Delta}^{x_0+\Delta} \phi (1 - 2p_s) dx \\ \tau_p \lambda c &= \lim_{\Delta \rightarrow 0} (\psi s'(h_s) p_s + s(h_s) \phi)_x \Big|_{x_0-\Delta}^{x_0+\Delta} + c(1 - p_s^+ - p_s^-) \\ \tau_p \lambda c &= s(h_s) \phi' \Big|_{x_0^-}^{x_0^+} + c(1 - p_s^+ - p_s^-) .\end{aligned}$$

Similarly, premultiplying (4.3) by x and integrate by parts, we obtain

$$0 = s(h_s) \phi \Big|_{x_0^-}^{x_0^+} .$$

Finally, premultiply (4.3) by x^2 and integrate by parts twice, we obtain

$$c = \frac{\psi(x_0)}{h'_s(x_0)} (p_s^+ - p_s^-) .$$

This last equation can be used to eliminate c , yielding the final jump conditions for the eigenvalue problem:

$$0 = s \phi' \Big|_{x_0^-}^{x_0^+} + \frac{\psi(x_0)}{h'_s(x_0)} (p_s^+ - p_s^-) (1 - p_s^+ - p_s^- - \tau_p \lambda) , \quad (4.4)$$

$$0 = s \phi \Big|_{x_0^-}^{x_0^+} , \quad (4.5)$$

$$0 = D_h \psi' \Big|_{x_0^-}^{x_0^+} + \frac{\psi(x_0)}{h'_s(x_0)} (p_s^+ - p_s^-) , \quad (4.6)$$

$$0 = \psi \Big|_{x_0^-}^{x_0^+} . \quad (4.7)$$

4.3 Jump Conditions via Linearization

We will now derive these equations by linearizing the matching conditions from the original system. Begin by noting that in the perturbed regime x_0 may vary with time. Because of this, we will need to linearize (3.5), rather than (3.1).

We linearize as before, taking $p(x, t) = p_s(x) + \phi(x) e^{\lambda t}$ and $h(x, t) = h_s(x) + \psi(x) e^{\lambda t}$. Since the location of the jump will change, we also perturb the interface location $x_0(t) = x_{0s} + \theta e^{\lambda t}$. As before, we split p and h into left and right components, denoted h_l, h_r , etc.

Expanding $h_l(x_0, t)$ and discarding higher order terms, we obtain

$$h_l(x_0, t) \approx 1 + e^{\lambda t} (\theta h'_{sl}(x_{0s}) + \psi_l(x_{0s})) .$$

We do the same for h_r , and substitute into (3.4). Recalling that $h'_{sl}(x_0) = h'_{sr}(x_0)$, this then yields

$$\psi_l(x_{0s}) = -\theta h'_{sl}(x_{0s}) = \psi_r(x_{0s}) .$$

Similarly, expanding $\partial_x h_l(x_0, t)$ yields

$$\partial_x h_l(x_0, t) \approx h'_{sl}(x_{0s}) + e^{\lambda t} (\theta h''_{sl}(x_0) + \psi'_l(x_0)) .$$

Substituting into (3.3) and simplifying yields

$$\psi' \Big|_{x_{0s}^-}^{x_{0s}^+} = \theta \frac{\alpha}{D_h} p_s \Big|_{x_{0s}^-}^{x_{0s}^+} .$$

Repeating this procedure for p and $\partial_x p$ and substitute into (3.5) and (3.2) we can derive

$$\begin{aligned} 0 &= s\phi \Big|_{x_{0s}^-}^{x_{0s}^+} , \\ 0 &= s\phi' \Big|_{x_{0s}^-}^{x_{0s}^+} + \theta \left(\tau_p \lambda (p_s^+ - p_s^-) + s p_s'' \Big|_{x_{0s}^-}^{x_{0s}^+} \right) . \end{aligned}$$

Eliminating θ , and reverting to the previous notation $x_{0s} \rightarrow x_0$, we recover

$$\begin{aligned} 0 &= s\phi' \Big|_{x_0^-}^{x_0^+} - \frac{\psi(x_0)}{h'_e(x_0)} \left(\tau_p \lambda (p_s^+ - p_s^-) + s p_s'' \Big|_{x_0^-}^{x_0^+} \right) , \\ 0 &= s\phi \Big|_{x_0^-}^{x_0^+} , \\ 0 &= D_h \psi' \Big|_{x_0^-}^{x_0^+} + \frac{\psi(x_0)}{h'_e(x_0)} p_s \Big|_{x_0^-}^{x_0^+} , \\ 0 &= \psi \Big|_{x_0^-}^{x_0^+} . \end{aligned}$$

At first glance, the first of these may appear different to the equations (4.4 – 4.7). However, using the fact that $s p_s'' = -p_s(1 - p_s)$, we can show that these are, in fact, equivalent.

4.4 Solutions to the Eigenvalue Problem for Large $s(h)$ Values

Having adequately set up the eigenvalue problem, all that remains is to pick a stationary solution and attempt to solve the system. We use the solution derived in section 3.3.

In keeping with our previous notation, we define ϕ_l , ϕ_r , etc. Recall that, to leading order, $p_{sl}(x) = p_{l0}$. Let $\omega_l = \frac{1}{D_+} (1 - 2p_{l0} - \tau_p \lambda)$. Solving (4.1) in the left of the domain, we obtain $\phi_l(x) = c_{l1} \cos(\sqrt{\omega_l}x)$, where c_{l1} is some constant to be determined. A similar solutions can be found for the right part of the domain.

Substituting into (4.2) yields a differential equations for ψ ;

$$\psi_l''(x) = -\frac{c_{l1}}{D_h} \cos(\sqrt{\omega_l}x) + \frac{1 + \lambda}{D_h} \psi_l(x) .$$

It has the following solution,

$$\psi_l(x) = \frac{c_{l1}}{1 + \lambda + D_h \omega_l} \cos(\sqrt{\omega_l}x) + c_{l2} \cosh \left(\sqrt{\frac{1 + \lambda}{D_h}} x \right) ,$$

where c_{l2} is a constant.

We can find similar solutions for the right of the domain. We substitute these solutions into equations (4.4–4.7). To simplify notation, let $k = \frac{p_e^+ - p_e^-}{h_e'(x_0)} (1 - p_e^+ - p_e^- - \tau_p \lambda)$. This results in the equations

$$\begin{aligned} 0 &= -D_- c_{r1} \sqrt{\omega_r} \sin(\sqrt{\omega_r}(x_0 - 1)) + D_+ c_{l1} \sqrt{\omega_l} \sin(\sqrt{\omega_l}x_0) \\ &\quad + k \left(\frac{c_{l1}}{1 + \lambda + D_h \omega_l} \cos(\sqrt{\omega_l}x_0) + c_{l2} \cosh \left(\sqrt{\frac{1 + \lambda}{D_h}} x_0 \right) \right) , \\ 0 &= D_- c_{r1} \cos(\sqrt{\omega_r}(x_0 - 1)) - D_+ c_{l1} \cos(\sqrt{\omega_l}x_0) , \\ 0 &= \frac{c_{r1}}{1 + \lambda + D_h \omega_r} \cos(\sqrt{\omega_r}(x_0 - 1)) + c_{r2} \cosh \left(\sqrt{\frac{1 + \lambda}{D_h}} (x_0 - 1) \right) \\ &\quad - \frac{c_{l1}}{1 + \lambda + D_h \omega_l} \cos(\sqrt{\omega_l}x_0) - c_{l2} \cosh \left(\sqrt{\frac{1 + \lambda}{D_h}} x_0 \right) , \end{aligned}$$

and

$$\begin{aligned}
0 = & -\frac{c_{r1}\sqrt{\omega_r}}{1+\lambda+D_h\omega_r} \sin(\sqrt{\omega_r}(x_0-1)) + c_{r2}\sqrt{\frac{1+\lambda}{D_h}} \sinh\left(\sqrt{\frac{1+\lambda}{D_h}}(x_0-1)\right) \\
& + \frac{c_{l1}\sqrt{\omega_l}}{1+\lambda+D_h\omega_l} \sin(\sqrt{\omega_l}x_0) - c_{l2}\sqrt{\frac{1+\lambda}{D_h}} \sinh\left(\sqrt{\frac{1+\lambda}{D_h}}x_0\right) \\
& + \frac{1}{D_h h'_e(x_0)} (p_e^+ - p_e^-) \left(\frac{c_{l1}}{1+\lambda+D_h\omega_l} \cos(\sqrt{\omega_l}x_0) + c_{l2} \cosh\left(\sqrt{\frac{1+\lambda}{D_h}}x_0\right) \right).
\end{aligned}$$

Written in matrix notation, we have

$$M \begin{bmatrix} c_{l1} \\ c_{r1} \\ c_{l2} \\ c_{r2} \end{bmatrix} = \begin{bmatrix} 0 \\ 0 \\ 0 \\ 0 \end{bmatrix}$$

where M is the matrix below, with $A_l = \frac{1}{1+\lambda+D_h\omega_l}$ (similarly for A_r), and $B = \sqrt{\frac{1+\lambda}{D_h}}$.

$$\begin{bmatrix} D_+\sqrt{\omega_l} \sin(\sqrt{\omega_l}x_0) + kA_l \cos(\sqrt{\omega_l}x_0) & -D_-\sqrt{\omega_r} \sin(\sqrt{\omega_r}(x_0-1)) & k \cosh(Bx_0) & 0 \\ -D_+ \cos(\sqrt{\omega_l}x_0) & D_- \cos(\sqrt{\omega_r}(x_0-1)) & 0 & 0 \\ -A_l \cos(\sqrt{\omega_l}x_0) & A_r \cos(\sqrt{\omega_r}(x_0-1)) & -\cosh(Bx_0) & \cosh(B(x_0-1)) \\ \sqrt{\omega_l}A_l \sin(\sqrt{\omega_l}x_0) & -\sqrt{\omega_r}A_r \sin(\sqrt{\omega_r}(x_0-1)) & -B \sinh(Bx_0) & B \sinh(B(x_0-1)) \\ +\frac{(p_e^+ - p_e^-)}{D_h h'_e(x_0)} A_l \cos(\sqrt{\omega_l}x_0) & & +\frac{(p_e^+ - p_e^-)}{D_h h'_e(x_0)} \cosh(Bx_0) & \end{bmatrix}$$

In order to have non-trivial solutions, we require that $\det M = 0$. Written in full, this determinant is

$$\begin{aligned}
\det M = & -D_+D_-\sqrt{\omega_r}B \cos(\sqrt{\omega_l}x_0) \sin(\sqrt{\omega_r}(x_0-1)) \sinh(B) \\
& + \frac{p_e^+ - p_e^-}{D_h h'_e(x_0)} D_+D_-\sqrt{\omega_r} \cos(\sqrt{\omega_l}x_0) \sin(\sqrt{\omega_r}(x_0-1)) \cosh(B(x_0-1)) \cosh(Bx_0) \\
& - A_r B D_+ k \cos(\sqrt{\omega_l}x_0) \cosh(Bx_0) \cos(\sqrt{\omega_r}(x_0-1)) \sinh(B(x_0-1)) \\
& - D_+ k \sqrt{\omega_r} A_r \cos(\sqrt{\omega_l}x_0) \cosh(Bx_0) \cosh(B(x_0-1)) \sin(\sqrt{\omega_r}(x_0-1)) \\
& + D_- D_+ \sqrt{\omega_l} B \cos(\sqrt{\omega_r}(x_0-1)) \sin(\sqrt{\omega_l}x_0) \sinh(B) \\
& - \frac{p_e^+ - p_e^-}{D_h h'_e(x_0)} D_- D_+ \sqrt{\omega_l} \cos(\sqrt{\omega_r}(x_0-1)) \sin(\sqrt{\omega_l}x_0) \cosh(B(x_0-1)) \cosh(Bx_0) \\
& + D_- k A_l B \cos(\sqrt{\omega_r}(x_0-1)) \cos(\sqrt{\omega_l}x_0) \sinh(B) \\
& + D_- k A_l B \cos(\sqrt{\omega_r}(x_0-1)) \cosh(Bx_0) \cos(\sqrt{\omega_l}x_0) \sinh(B(x_0-1)) \\
& + D_- k \sqrt{\omega_l} A_l \cos(\sqrt{\omega_r}(x_0-1)) \cosh(Bx_0) \cosh(B(x_0-1)) \sin(\sqrt{\omega_l}x_0).
\end{aligned}$$

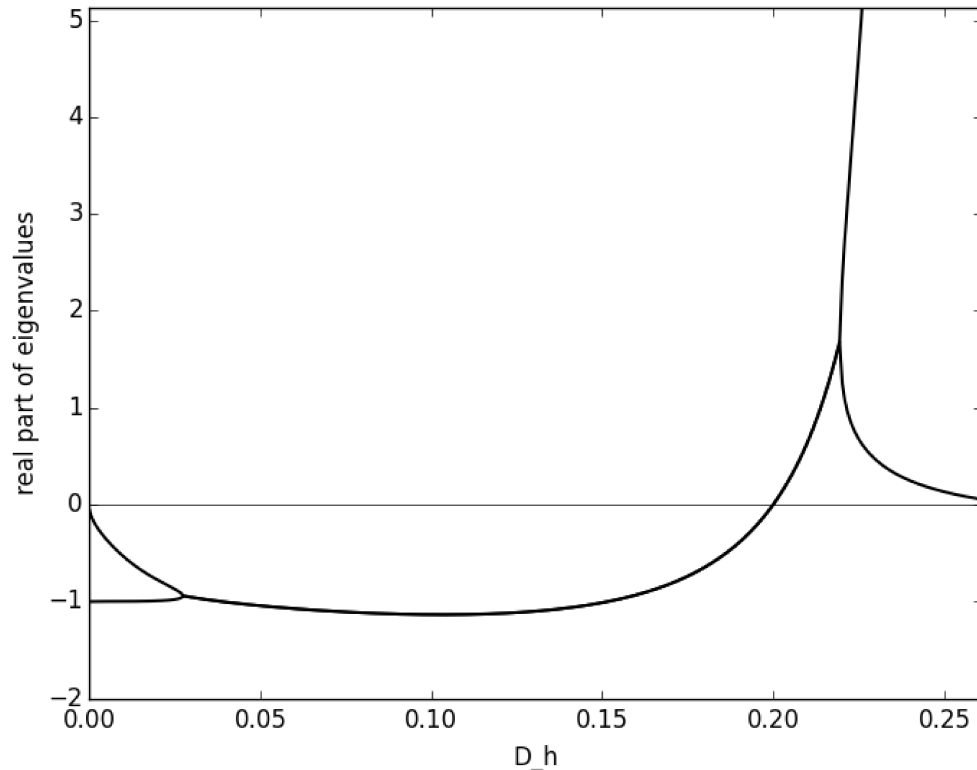


Figure 4.1: Plotting the real part of the first two eigenvalues as a function of D_h , with $s_0 = 0.5$. Notice as D_h becomes large, the first eigenvalue grows very quickly. This apparent asymptote corresponds to the onset of non-existence of single-jump solutions. At intermediate D_h values the first two roots become a complex pair, and the system undergoes a Hopf bifurcation. For small D_h values, the first two roots are again real, but remain negative.

Thus, the eigenvalue problem in the case where $s(h)$ is large reduces to finding the roots of this expression. While this is analytically intractable, we can nevertheless find roots numerically, tracking the movement of the first eigenvalues (see Figure 4.1). This analysis reveals a Hopf bifurcation. Simulations at appropriate parameter values reveal the expected oscillatory behaviour (see Figure 4.2).

These calculations can be further verified by solving the eigenvalue problem numerically. If we take s to be a sufficiently sharp sigmoid, rather than a piecewise constant function, then the PDEs (4.2) and (4.3) can be discretized using standard techniques. This can be done using specialized software (such as FlexPDE), or coded from scratch. We will briefly outline one way in which this might be done.

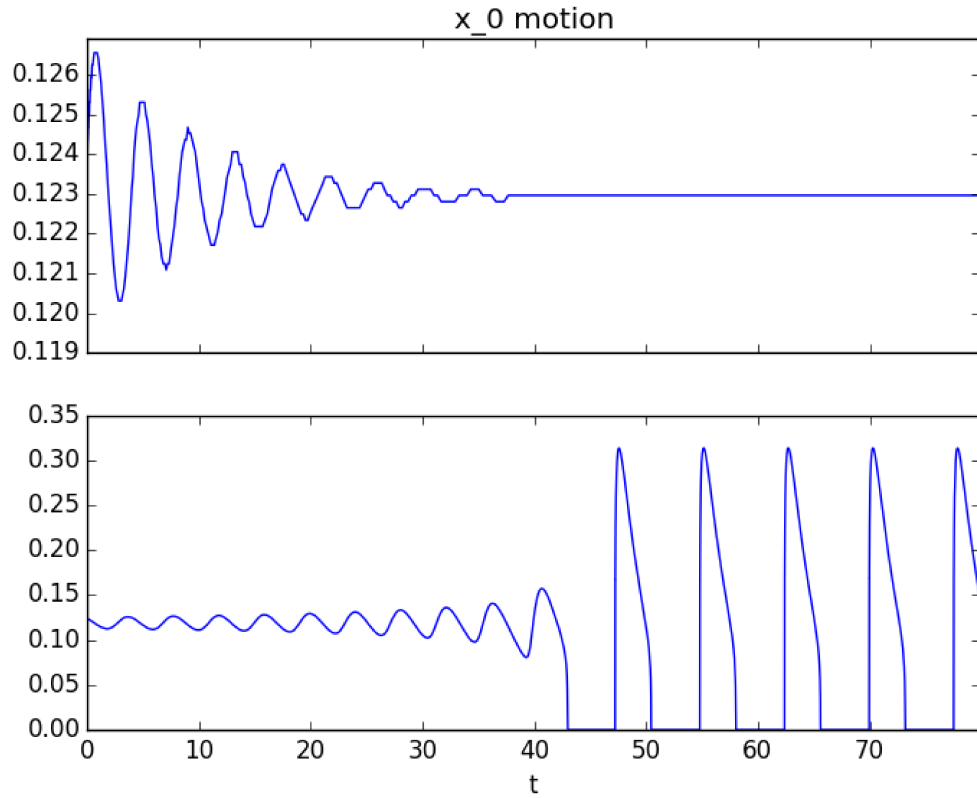


Figure 4.2: Plots comparing the motion of x_0 in the linearly stable ($D_h = 0.199$, top) and linearly unstable ($D_h = 0.202$, bottom) regimes, with $D_+ = 500$ and $D_- = 1000$ in both cases, and $s(h)$ approximated by a sharp sigmoid curve. In each plot, the steady-state solution was perturbed, and the location of x_0 tracked as the solution evolved. In the stable case, the location of x_0 exhibits damped oscillations consistent with the predicted eigenvalues. In the unstable case, the oscillations grow until x_0 drifts to the edge of the domain, at which point the solution collapses to an approximately constant and homogeneous profile ($t \approx 45$). This is followed by repeated spontaneous emergence of structure via Turing instability, punctuated by collapse to a nearly constant solution.

To discretize the problem, one first discretizes the domain; we translate the problem from the interval $[0, 1]$ to some finite collection of equidistant points $0 = x_1 < x_2 < \dots < x_n = 1$. All the relevant functions, p , h , s , ϕ , and ψ , are replaced by their discrete counterparts, and the differential operators are replaced by matrices (there are many ways to do with, but the most straightforward method is to use finite differences to approximate derivatives, using the no-flux boundary conditions to handle the values at the edges of the domain). This converts the problem to a matrix eigenvalue problem where the matrix in question is very sparse.

4.5 Revisiting Stability in the Small D_h , $\tau_p = 0$ Regime

While the equation governing the eigenvalues in the large s case is generally intractable, we should expect it to simplify considerably when D_h is small and $\tau_p = 0$. After all, we have already shown that this limiting case is stable and has a relatively simple eigenvalue. With this in mind, we attempt to simplify $\det(M)$, in the hopes that we recover the same result as before.

We begin by approximating the cosh and sinh terms by a suitable exponential to obtain

$$\begin{aligned} \det(M) \approx & -\frac{1}{2} D_+ D_- \sqrt{w_r} B \cos(\sqrt{w_l} x_0) \sin(\sqrt{w_r} (x_0 - 1)) e^B \\ & + \frac{1}{4} \frac{(p_{r0} - p_{l0}) D_+ D_- \sqrt{w_r} \cos(\sqrt{w_l} x_0) \sin(\sqrt{w_r} (x_0 - 1)) e^B}{D_h h_x} \\ & + \frac{1}{4} A_r B D_+ k \cos(\sqrt{w_l} x_0) \cos(\sqrt{w_r} (x_0 - 1)) e^B \\ & - \frac{1}{4} D_+ k \sqrt{w_r} A_r \cos(\sqrt{w_l} x_0) \sin(\sqrt{w_r} (x_0 - 1)) e^B \\ & + \frac{1}{2} D_+ D_- \sqrt{w_l} B \cos(\sqrt{w_r} (x_0 - 1)) \sin(\sqrt{w_l} x_0) e^B \\ & - \frac{1}{4} \frac{(p_{r0} - p_{l0}) D_+ D_- \sqrt{w_l} \cos(\sqrt{w_r} (x_0 - 1)) \sin(\sqrt{w_l} x_0) e^B}{D_h h_x} \\ & + \frac{1}{4} D_- k A_l B \cos(\sqrt{w_r} (x_0 - 1)) \cos(\sqrt{w_l} x_0) e^B \\ & + \frac{1}{4} D_- k \sqrt{w_l} A_l \cos(\sqrt{w_r} (x_0 - 1)) \sin(\sqrt{w_l} x_0) e^B . \end{aligned}$$

We then use the fact that D_+ and D_- are large to approximate the cos and sin terms by a first order Taylor expansion. This yields

$$\begin{aligned}
\det(M) &\approx -\frac{1}{2}D_+B(1-2p_{r0})(x_0-1)e^B + \frac{1}{4}\frac{(p_{r0}-p_{l0})D_+(x_0-1)e^B}{D_h h_x}(1-2p_{r0}) \\
&\quad + \frac{1}{4}A_r B D_+ k e^B - \frac{1}{4}s_0 k A_r e^B(1-2p_{r0})(x_0-1) \\
&\quad + \frac{1}{2}D_-B(1-2p_{l0})x_0 e^B - \frac{1}{4}\frac{(p_{r0}-p_{l0})D_-x_0 e^B}{D_h h_x}(1-2p_{l0}) \\
&\quad + \frac{1}{4}D_-k A_l B e^B + \frac{1}{4}\frac{k A_l e^B x_0}{s_0}(1-2p_{l0}) .
\end{aligned}$$

Recall that, since $\tau_p = 0$, we obtain the following simplification:

$$\begin{aligned}
A_l &= \frac{1}{1+\lambda + D_h \omega_l} \\
&= \frac{1}{1+\lambda + D_h \left(\frac{1}{D_+}(1-2p_{l0})\right)} \\
&\approx \frac{1}{1+\lambda} .
\end{aligned}$$

Similarly, $A_r \approx \frac{1}{1+\lambda}$. We also find $k = \frac{p_{r0}-p_{l0}}{h'_s(x_0)}(1-p_{l0}-p_{r0})$. From the results from section 3.3, we can also show that $h'_s(x_0) \approx \sqrt{\frac{1}{D_h}(1-p_{l0})}$ when D_h is small. Thus

$$k \approx \sqrt{D_h} \frac{p_{r0}-p_{l0}}{1-p_{l0}}(1-p_{l0}-p_{r0}) .$$

Also recall from proposition 2 that $p_{l0} = \frac{2}{s_0+1}$, and $p_{r0} = \frac{2s_0}{s_0+1}$ in the small D_h regime. Substitution into the equation above and simplifying yields

$$k \approx -2\sqrt{D_h} .$$

Finally, recall that $x_0 = \frac{s_0}{s_0+1}$. Substituting all of this into the equation for $\det(M)$ yields

$$\begin{aligned}
\det(M) &\approx -\frac{1}{2}D_+\sqrt{\frac{1+\lambda}{D_h}}\left(1-2\frac{2s_0}{s_0+1}\right)\left(\frac{s_0}{s_0+1}-1\right)e^B \\
&+ \frac{1}{4}\frac{\left(\frac{2s_0}{s_0+1}-\frac{2}{s_0+1}\right)D_+\left(\frac{s_0}{s_0+1}-1\right)e^B}{D_h\sqrt{\frac{1}{D_h}}\left(1-\frac{2}{s_0+1}\right)}\left(1-2\frac{2s_0}{s_0+1}\right) \\
&+ \frac{1}{4}\frac{1}{1+\lambda}\sqrt{\frac{1+\lambda}{D_h}}D_+(-2\sqrt{D_h})e^B \\
&- \frac{1}{4}s_0(-2\sqrt{D_h})\frac{1}{1+\lambda}e^B\left(1-2\frac{2s_0}{s_0+1}\right)\left(\frac{s_0}{s_0+1}-1\right) \\
&+ \frac{1}{2}D_-\sqrt{\frac{1+\lambda}{D_h}}\left(1-2\frac{2}{s_0+1}\right)\frac{s_0}{s_0+1}e^B \\
&- \frac{1}{4}\frac{\left(\frac{2s_0}{s_0+1}-\frac{2}{s_0+1}\right)D_-\frac{s_0}{s_0+1}e^B}{D_h\sqrt{\frac{1}{D_h}}\left(1-\frac{2}{s_0+1}\right)}\left(1-2\frac{2}{s_0+1}\right) \\
&+ \frac{1}{4}D_+(-2\sqrt{D_h})\frac{1}{1+\lambda}\sqrt{\frac{1+\lambda}{D_h}}e^B + \frac{1}{4}\frac{(-2\sqrt{D_h})\frac{1}{1+\lambda}e^B\frac{s_0}{s_0+1}}{s_0}\left(1-2\frac{2}{s_0+1}\right) \\
&= -\frac{1}{2}\frac{e^B}{\sqrt{D_h}(s_0+1)^2(1+\lambda)}\left(\left((s_0+1)^2(D_++D_-)\sqrt{D_h}\right.\right. \\
&\quad \left.\left.+ 3(-1/3D_-s_0^2+(D_++D_-)s_0-D_+/3)(1+\lambda)\right)\sqrt{1+\lambda}\right. \\
&\quad \left.+ ((1+\lambda)D_- - 3D_h)s_0^2 + ((-3\lambda-3)D_+ + (-3\lambda-3)D_- + 2D_h)s_0\right. \\
&\quad \left.+ (1+\lambda)D_+ - 3D_h\right) \\
&= -\frac{1}{2}\frac{e^B}{\sqrt{D_h}(s_0+1)^2(1+\lambda)}\left(\left((s_0+1)D_-\left(\sqrt{D_h}(s_0+1)^2+2s_0(1+\lambda)\right)\sqrt{1+\lambda}\right.\right. \\
&\quad \left.\left.+ ((-2\lambda-2)D_- - 3D_h)s_0^2 + ((-2\lambda-2)D_- + 2D_h)s_0 - 3D_h\right)\right).
\end{aligned}$$

Thus, the problem now reduces to solving

$$\begin{aligned}
0 &= (s_0+1)D_-\left(\sqrt{D_h}(s_0+1)^2+2s_0(1+\lambda)\right)\sqrt{1+\lambda} \\
&\quad + ((-2\lambda-2)D_- - 3D_h)s_0^2 + ((-2\lambda-2)D_- + 2D_h)s_0 - 3D_h.
\end{aligned}$$

Since D_h is small, we can instead solve the slightly simpler equation

$$\begin{aligned}
0 &= (s_0+1)D_-\left(\sqrt{D_h}(s_0+1)^2+2s_0(1+\lambda)\right)\sqrt{1+\lambda} \\
&\quad + (-2\lambda-2)D_-s_0^2 + (-2\lambda-2)D_-s_0.
\end{aligned}$$

Which has three roots:

$$\begin{aligned}\lambda &= -1, \\ \lambda &= \frac{1 - \sqrt{D_h} (s_0 + 1)^2 - \sqrt{s_0^2 - 2\sqrt{D_h} (s_0 + 1)^2 s_0 - s_0}}{2s_0}, \\ \lambda &= \frac{1 - \sqrt{D_h} (s_0 + 1)^2 + \sqrt{s_0^2 - 2\sqrt{D_h} (s_0 + 1)^2 s_0 - s_0}}{2s_0}.\end{aligned}$$

Finally, expanding $\sqrt{s_0^2 - 2\sqrt{D_h} (s_0 + 1)^2 s_0} \approx s_0 - \sqrt{D_h} (s_0 + 1)^2$, we find that these two last roots are $\lambda \approx -1$ and $\lambda \approx -\sqrt{D_h} \frac{(s_0 + 1)^2}{s_0}$. Thus, we recover the result from section 3.4. Notice also that in figure 4.1 the second eigenvalue goes to -1 as $D_h \rightarrow 0$, as predicted by this analysis.

Chapter 5

Discussion

We have demonstrated that the PDE model proposed in [17] does indeed admit non-constant stationary solutions. These solutions are periodic and contain jump discontinuities, similar to a square wave. We focused our attention on solutions with a single jump discontinuity, and derived, assuming the diffusion of AHL was small, an equation of motion for a discontinuity that is not at equilibrium. The equation of motion was able to predict results from numerical simulations. From this equation of motion, we were able to deduce that such solutions are stable when diffusion of bacteria is large.

We then turned our attention to stability in a more general case (lifting the requirement that AHL diffusion be small, but maintaining the requirement that there be only one jump discontinuity), and derived an associated eigenvalue problem. We then showed that this eigenvalue problem was equivalent to finding the roots of a transcendental equation. Solving this equation numerically, we demonstrated the existence of a Hopf bifurcation, which was then confirmed in simulation. Finally, we showed that the transcendental equation was able to reproduce the eigenvalues predicted by the equation of motion.

This behaviour is markedly different from that described in [17]. Though they used the same model, their choice of parameters were such that only transient patterns could be created; any structure that emerged eventually collapsed to the trivial constant state. To obtain the type of sustained pattern observed in experiment, their group developed a three-component PDE model [13]. Most of the difference in behaviour can be attributed to the nature of the function $s(h)$. In this thesis, we chose $s(h)$ to ensure that the system exhibited a Turing instability, and this choice ensured that any observed steady states would be non-constant. It remains an open question

whether or not such stable steady states exist for more generic $s(h)$.

This work provides further evidence that non-linear diffusion can act as a pattern generation mechanism. While the methods used were largely ad hoc and relied heavily on approximation, the results obtained agree with numerical simulation and display internal consistency (several of the results can be derived via multiple methods). It is our hope that these results might act as a catalyst for further experiments, or as a starting point for anyone who wishes to pursue a more rigorous analysis.

A number of open problems remain. How does one characterize the stability of solutions with multiple discontinuities? What can be said of the case where $\tau_p \neq 0$? Can one derive similar results where $s(h)$ is a smooth curve? Numerical simulations show that similar patterns form even when $s(h)$ is a sigmoid curve with a gradual slope. Finally, what happens when we extend this model to more than one spatial dimension? In the experiments that motivated the creation of this model, researchers observed stable stripes and concentric circles, and preliminary simulations show that the model has a natural tendency to develop spots when evolved from a perturbed homogeneous state. We hope to address these questions in future work.

Bibliography

- [1] E. Ben-Jacob, I. Cohen, and H. Levine, “Cooperative self-organization of microorganisms,” *Advances in Physics*, vol. 49, no. 4, pp. 395–554, 2000.
- [2] D. Horstmann *et al.*, “From 1970 until present: the keller-segel model in chemotaxis and its consequences,” 2003.
- [3] J. A. Sherratt, “Wavefront propagation in a competition equation with a new motility term modelling contact inhibition between cell populations,” in *Proceedings of the Royal Society of London A: Mathematical, Physical and Engineering Sciences*, vol. 456, no. 2002. The Royal Society, 2000, pp. 2365–2386.
- [4] D. del Castillo-Negrete, B. Carreras, and V. Lynch, “Front propagation and segregation in a reaction–diffusion model with cross-diffusion,” *Physica D: Nonlinear Phenomena*, vol. 168, pp. 45–60, 2002.
- [5] R. Ruiz-Baier and C. Tian, “Mathematical analysis and numerical simulation of pattern formation under cross-diffusion,” *Nonlinear Analysis: Real World Applications*, vol. 14, no. 1, pp. 601–612, 2013.
- [6] C. Tian, Z. Lin, and M. Pedersen, “Instability induced by cross-diffusion in reaction–diffusion systems,” *Nonlinear Analysis: Real World Applications*, vol. 11, no. 2, pp. 1036–1045, 2010.
- [7] G. Gambino, M. C. Lombardo, and M. Sammartino, “Turing instability and traveling fronts for a nonlinear reaction–diffusion system with cross-diffusion,” *Mathematics and Computers in Simulation*, vol. 82, no. 6, pp. 1112–1132, 2012.
- [8] J. Müller and W. van Saarloos, “Morphological instability and dynamics of fronts in bacterial growth models with nonlinear diffusion,” *Physical Review E*, vol. 65, no. 6, p. 061111, 2002.
- [9] P. Rosenau, “Reaction and concentration dependent diffusion model,” *Physical review letters*, vol. 88, no. 19, p. 194501, 2002.
- [10] B. Gilding and R. Kersner, “A fisher/kpp-type equation with density-dependent diffusion and convection: travelling-wave solutions,” *Journal of Physics A: Mathematical and General*, vol. 38, no. 15, p. 3367, 2005.
- [11] K. Kawasaki, A. Mochizuki, M. Matsushita, T. Umeda, and N. Shigesada, “Modeling spatio-temporal patterns generated by bacillus subtilis,” *Journal of Theoretical Biology*, vol. 188, no. 2, pp. 177–185, 1997.

- [12] M. B. Miller and B. L. Bassler, “Quorum sensing in bacteria,” *Annual Reviews in Microbiology*, vol. 55, no. 1, pp. 165–199, 2001.
- [13] C. Liu, X. Fu, L. Liu, X. Ren, C. K. Chau, S. Li, L. Xiang, H. Zeng, G. Chen, L.-H. Tang *et al.*, “Sequential establishment of stripe patterns in an expanding cell population,” *Science*, vol. 334, no. 6053, pp. 238–241, 2011.
- [14] F. Farrell, M. Marchetti, D. Marenduzzo, and J. Tailleur, “Pattern formation in self-propelled particles with density-dependent motility,” *Physical review letters*, vol. 108, no. 24, p. 248101, 2012.
- [15] J. Tailleur and M. Cates, “Statistical mechanics of interacting run-and-tumble bacteria,” *Physical review letters*, vol. 100, no. 21, p. 218103, 2008.
- [16] M. Cates, D. Marenduzzo, I. Pagonabarraga, and J. Tailleur, “Arrested phase separation in reproducing bacteria creates a generic route to pattern formation,” *Proceedings of the National Academy of Sciences*, vol. 107, no. 26, pp. 11 715–11 720, 2010.
- [17] X. Fu, L.-H. Tang, C. Liu, J.-D. Huang, T. Hwa, and P. Lenz, “Stripe formation in bacterial systems with density-suppressed motility,” *Physical review letters*, vol. 108, no. 19, p. 198102, 2012.
- [18] V. Kenkre and M. Kuperman, “Applicability of the fisher equation to bacterial population dynamics,” *Physical Review E*, vol. 67, no. 5, p. 051921, 2003.

Appendix A

FlexPDE Code

```
COORDINATES CARTESIAN1 { coordinate system, 1D,2D,3D, etc }
VARIABLES { system variables }
h (threshold=1e-20)
p (threshold=1e-20) { choose your own names }
SELECT { method controls }
errlim=1e-5
!TERRIM=10e-1
!PREFER_STABILITY

DEFINITIONS { parameter definitions }
L=1.
Tmax=10
tau = 1
Sp=1000;
Sm=500;
D.h=0.05

eps=0.001
S=(tanh((1-h)/eps)+1)*(Sp-Sm)/2+Sm;
! when running for the first time, remove the following line and change initial conditions
transfer ('../x.ic', p00,h00)

INITIAL VALUES
h=h00!+0.001*RANDOM(x)
p=p00!+0.001*RANDOM(x)

EQUATIONS { PDE's, one for each variable }
h: dt(h)=D.h*dxx(h)+p-h
p: tau*dt(p)=dxx(S*p)+p*(1-p)

! CONSTRAINTS { Integral constraints }
BOUNDARIES { The domain definition }
REGION 1 { For each material region }
START(0) { Walk the domain boundary }
point natural(h)=0
point natural(p)=0

line to (L)

TIME 0 TO Tmax { if time dependent }
MONITORS { show progress }
for cycle=1
elevation(h, p) from (0) to (L) !export format "#x#b#1#b#2" file="plotInfo.txt"
plots
for t=0 by Tmax/50 to Tmax
elevation(p) from (0) to (L) export format "#x#b#1" file="plot.txt"
histories
history(GLOBALMIN_X((h-1)^2)) EXPORT format "#t#r#i" file="interfaceMotion.txt"

END
```